Micro/Nanostructure Engineering of Epitaxial Piezoelectric α-quartz Thin Films on Silicon

*Q. Zhang[1, 2 γ], D. Sánchez-Fuentes[1 γ], R. Desgarceaux[1 γ], P. Escofet-Majoral[1], J. Oró-soler[2], J. Gazquez[2], G. Larrieu[3], B. Charlot[1], A. Gomez[2], M. Gich[2], A. Carretero-Genevrier[1]**

1. David Sánchez-Fuentes, Rudy Desgarceaux, Pau Escofet-Majoral, Dr. Benoit Charlot, Dr. Adrian Carretero-Genevrier
Institut d'Electronique et des Systemes (IES), CNRS, Université de Montpellier, 860 Rue de Saint Priest 34095 Montpellier, France
2. Qianzhe Zhang, Andres Gomez, Dr. Judith Oró-soler, Dr. Jaume Gazquez, Dr. Marti Gich
Institut de Ciència de Materials de Barcelona ICMAB, Consejo Superior de Investigaciones Científicas CSIC, Campus UAB 08193 Bellaterra, Catalonia, Spain
3. Guilliem Larrieu
LAAS-CNRS, Université de Toulouse, CNRS, INP, 7 av. Colonel Roche, 31031Toulouse, France

γ These authors contributed equally to this work
E-mail: carretero@ies.univ-montp2.fr,

Keywords: Quartz, silicon, epitaxial growth, thin films, piezoelectricity, nanostructuration

Abstract

The monolithic integration of sub-micron quartz structures on silicon substrates is a key issue for the future development of piezoelectric devices as prospective sensors with applications based on the operation in the high frequency range. However, to date it has not been possible to make existing quartz manufacturing methods compatible with integration on silicon and structuration by top down lithographic techniques. Here we report unprecedented large-scale fabrication of ordered arrays of piezoelectric epitaxial quartz nanostructures on silicon substrates by the combination of soft-chemistry and three lithographic techniques: (i) laser transfer lithography, (ii) soft nanoimprint lithography on Sr-doped SiO_2 sol-gel thin films and (iii) self-assembled $SrCO_3$ nanoparticles reactive nanomasks. Epitaxial α-quartz nanopillars with different diameters (from 1 μm down to 50 nm) and heights (up to 2000 nm) were obtained. This work demonstrates the complementarity of soft-chemistry and top-down lithographic techniques for the patterning of epitaxial quartz thin films on silicon while preserving its epitaxial crystallinity and piezoelectric properties. These results open up the opportunity to develop a cost-effective on-chip integration of nanostructured piezoelectric α-quartz MEMS with enhanced sensing properties of relevance in different fields of application.

1
2
3
4
5
6
7
8
9
10
11
12
13
14
15
16
17
18
19
20
21
22
23
24
25
26
27
28
29
30
31
32
33
34
35
36
37
38
39
40
41
42
43
44
45
46
47
48
49
50
51
52
53
54
55
56
57
58
59
60

1. Introduction.

Piezoelectric materials are present in most electronic circuits and devices, where they play key functions as high frequency stable oscillators and efficient inertial sensors for distance, movement and acceleration detection. In this context, the integration of high quality epitaxial piezoelectric films and nanostructures on silicon is a milestone towards the expansion of novel devices with the traditional Si-based complementary metal-oxide-semiconductor (CMOS) technology[1]. In addition, the advances in micro and nanofabrication technologies open the door to a large scale integration of miniaturized piezoelectric materials and to the implementation of innovative electromechanical devices with nanosized moving parts which could enable new sensor sensor applications in electronics, biology and medicine[2-4].

In particular, α-quartz is widely used for electronic applications: its piezoelectric properties allow for an excellent frequency control in oscillators and the production of very selective filters[5]. Since the eigen frequency of the quartz crystal is very sensitive to changes of its mass or acceleration, this material is extremely convenient to implemented micro-resonators for sensing applications (strength, humidity, acceleration, etc.)[6, 7]. However, α-quartz and other piezoelectric sensing materials displaying extremely large quality factor ($Q > 10^6$)[8], high temperature stability and very low phase noise are only available as bulk single crystals. For this reason, all these excellent sensing materials can only be configured as high performance transducers through direct bulk micromachining or hybrid integration methods[9]

Nowadays, the lowest achievable thickness of quartz crystals is about 10 μm and 100 μm in diameter. In turn, this also limits the working frequencies of the transducers because the wavelength of the resonance frequency roughly corresponds to half of the of the crystal thickness. So far, only a few works reported sub-micron patterned surfaces in bulk crystals[10-12], such as those prepared on

1
2
3 quartz by Laser Interference Lithography[13] and by Faraday cage angled-etching technique[14, 15] or
4
5 lithium niobiate nanostructures synthetized by focused ion beam (FIB) technology[16].
6
7
8 We recently developed the direct and *bottom-up* integration of epitaxial α-quartz thin films on
9
10 silicon substrate by chemical solution deposition (CSD)[17, 18], which overcomes the aforementioned
11
12 limitations. The method relies on the thermal devitrification and crystallization of dip-coated
13
14
15 mesoporous silica films, assisted by strontium alkaline earth cation in amphiphilic molecular
16
17 templates[17]. This new approach opens the door for developing efficient quartz-based piezoelectrics
18
19 devices engineered from widely available and non-toxic compounds using industrially scalable
20
21
22 methods.
23
24 In the present work, we have taken advantage of an improved evolution of this chemical route[19]
25
26 and we have combined it with a set of *top-down* lithography techniques to fabricate large scale
27
28
29 epitaxial nanopatterned quartz thin films on silicon substrates with controllable nano and
30
31 microstructures. This work is, to our knowledge, one of the first example which shows the
32
33 possibility of engineering the integration of patterned quartz thin films on silicon, a step which
34
35
36 precedes the production of nanostructured microelectromechanical systems, as previously
37
38 highlighted[20]. By engineering on silicon α-quartz films with thicknesses between 200 nm and 1
39
40 μm, which are between 10 and 50 times thinner than those obtained by top down technologies on
41
42
43 bulk crystals, one can expect devices operating at ten to fifty-fold higher resonance frequencies[14].
44
45 In addition to the film thinness, the coherent Si/quartz interface combined now with a controlled
46
47 1D patterning may enable the fabrication of ultra-sensitives quartz devices capable to measuring
48
49
50 tiny masses ore forces through a variation in the resonant frequency[21]. For instance, micro- and
51
52 nanoelectromechanical (MEMS / NEMS) based on ultra-sensitive biocompatible nanostructured
53
54 resonant structures like cantilevers, bridges or plates would be highly beneficial for biochemical
55
56
57 sensing, allowing to study the molecular interactions of many cellular processes which are assisted
58
59
60

by topography (e.g. cell migration, membrane trafficking and signaling)[22-24]. Another biomedical application which could benefit from the fabrication of 1D piezoelectric nanostructures is the electromechanical stimulation of neurons or for other tissues in order to promote regeneration (e.g. neuronal guidance)[25, 26]. Likewise, marine piezoelectric sensors based on engineered quartz micro topographies as a natural defense system against bacterial colonization or formation of biofilms could be another important application derived from this work. This is supported by the fact that micro and nanostructured surfaces act as a protecting system against bacterial colonization or biofilm that will preserve the efficiencies and performance of the piezoelectric device[27]. The future development of biocompatible piezoelectric sensors employing 1D-nano and microstructures can reach a deep impact on healthcare and safety, thereby playing a more and more important role in the near future.

2. Results and discussions

Aiming to produce 1D arrays of pillars on epitaxial α-quartz thin films by silicon micromachining, we have tested the suitability of lithographic techniques such as laser transfer lithography technique[28], Soft nanoimprint lithography[29] and a novel plasma-assisted self-assembled $SrCO_3$ nanoparticles reactive nanomask etching. Such procedures do not require any lithographic mask and yield a large scale and precise control of epitaxial quartz nanostructures (see Fig. 1).

1
2
3
4
5
6
7
8
9
10
11
12
13
14
15
16
17
18
19
20
21
22
23
24
25
26
27
28
29
30

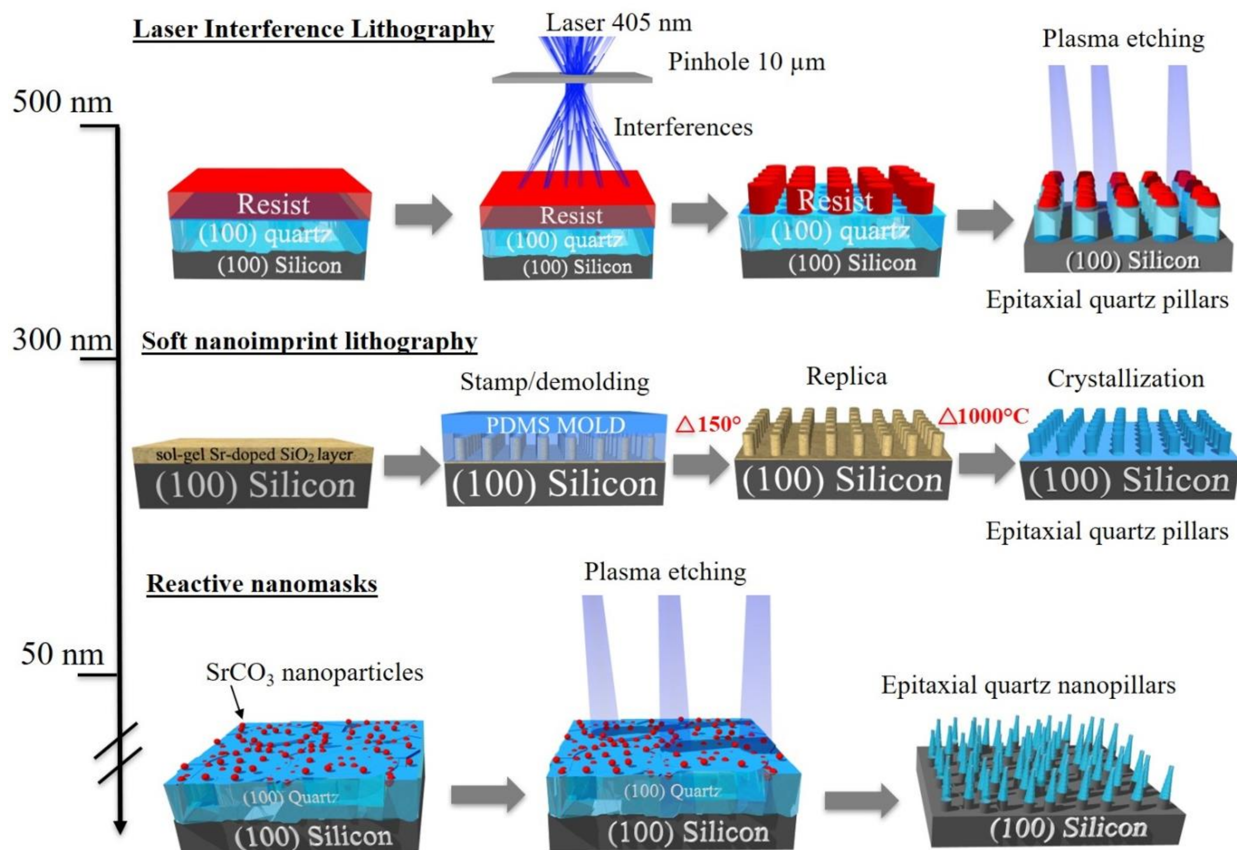

31
32
33
34

Fig. 1. Schematics summarizing the key steps applied to lithographic patterns on epitaxial quartz. The vertical axis indicates the typical dimensions of the lateral features achieved by the different techniques.

35
36
37
38
39
40
41
42
43
44
45
46
47
48
49
50
51
52

To evaluate the crystal stability of quartz under an anisotropic plasma etching, we initially produced photolithographic patterns consisting of 5 µm width lines on 300 nm thick films, which did not undergo amorphization during the process (see Fig.SI1). This was confirmed by 2D X-ray diffraction (XRD) and Piezo-response Force Microscopy (PFM) on micro-photolithographed samples. The XRD analysis revealed the same (100) α-quartz out of plane texture that the films had before the etching process and PFM measurements indicated that the piezoelectricity of micro patterned quartz films was preserved (see Fig.SI1 d and e), with the piezoelectric coefficient (d_{33}) being comparable to that of the quartz bulk material (i.e. 1.5 and 3.5 pm/V)[30-32].

53
54
55
56
57
58
59
60

1
2
3
4
5
6
7
8
9
10
11
12
13
14
15
16
17
18
19
20
21
22
23
24
25
26
27
28
29
30
31
32
33
34
35
36
37
38
39
40
41
42
43
44
45
46
47
48
49
50
51
52
53
54
55
56
57
58
59
60

2.1. Direct patterning of epitaxial piezoelectric quartz thin films by Laser Interference Lithography.

Next, we used Laser Interference Lithography (LIL, also known as holographic lithography) to obtain direct sub-micro patterned epitaxial quartz films. LIL process is a top-down fabrication technique that is currently used to selectively pattern single crystals into vertical nanocolumn arrays[13]. This technique allows generating arrays of lines or dots in a photoresist film from an interference pattern generated by a UV laser over cm^2 surfaces and with pitches ranging between 400 nm up to 2400 nm (see Fig. 2). The mask-less exposure of the photoresist layer together with two or more coherent light beams offers a simple, and large-area nanolithography technique[28].

To produce 1D epitaxial α-quartz nanocolumns with different aspects ratios it is essential to increase the film thicknesses towards the micron range. To this aim we used a multi-layer deposition approach consisting in the sequential deposition and consolidation of several gel layers, followed by a final annealing treatment to induce the epitaxial growth of α-quartz. Figure 2a shows a first nano lithographic pattern on a 600 nm thick epitaxial quartz thin films on (100) silicon substrate using LIL lithography. Low resolution Scanning Electron Microscopy image (SEM) displays a network of quartz columns with a precise control over their diameter, height and position. The Transmission Electron Microscopy image of the α-quartz/Si interface in a 600 nm height pillar and its corresponding Electron Diffraction pattern confirms that the crystalline quality of epitaxial α-quartz has been preserved during the LIL and RIE etching process (see Fig.2b).

The d_{33} piezoelectric coefficient estimated by PFM on the quartz columns was compared with the values obtained in the films before the lithographic process using an alternative PFM mode, direct piezoelectric force microscopy (DPFM), recently developed by A. Gomez *et al.*[33] (see Fig. SI2 and Fig. 2c). The piezoelectric coefficients obtained from both measurements are similar and comparable to that of the quartz bulk material[30] (i.e. $d_{33(PFM)} = 2\pm0.5$ pm/V and $d_{33(DPFM)} = 4\pm2$

1
2
3
4
5
6
7
8
9
10
11
12
13
14
15
16
17
18
19
20
21
22
23
24
25
26
27
28
29
30
31
32
33
34
35
36
37
38
39
40
41
42
43
44
45
46
47
48
49
50
51
52
53
54
55
56
57
58
59
60

pC/N) confirming that the piezoelectric functionality of the columns is preserved (see Fig. 2d and S2, respectively). Notice that all DPFM measurements were compared with a reference based on a commercial ferroelectric Periodically Poled Lithium Niobate sample (see Fig. SI3 for more details). The graphical representation in Figure 2d illustrates the control of quartz columns heights (up to 800 nm) as a function of the number of depositions of SiO_2 layers. Fig. S4a presents a series of FEGSEM images corresponding to the cross sections of quartz films consisting of 1 up to 5 layers before the lithographic process. Notice that the thicknesses of the different multilayer films match the heights of the quartz columns obtained after RIE process which are represented in figure 2d. From the XRD measurements of Fig. S4b we can see that all the films present the usual α-quartz (100) out of plane texture and that the intensity of the reflections is proportional to the number of layers of the film. This demonstrates that with the multi-layer approach it is possible to control the height of the columns produced by LIL while maintaining the crystallinity and crystal orientation. In Fig. 2e, the long range θ-2θ XRD pattern of a 5-layer film after lithography confirms the (100) out of plane texture of α-quartz with no supplementary peaks from other reflections or polycrystallinity signals. The pole figure presented in the inset shows that the (100) α-quartz [100]*‖(100) Si [100]* epitaxial relationship previously observed in films[17] has been preserved. By combining our multi-layer deposition approach with LIL lithography, we have produced high aspect ratio epitaxial quartz columns with micrometric heights from dip-coated films. This was possible because the multi-layer deposition approach allows circumventing the issues that can appear when preparing increasingly thicker films as for instance the lack of film homogeneity, as we found for withdrawal speeds above 15 mm/s (i.e. for film thickness above 420 nm) or the cracking which has been reported to originate from the development of lateral tensile stresses during the densification of the layers[34]. A key step to overcome this obstacle was performing a

thermal treatment to consolidate the gel layer (450ºC for 10 min in air atmosphere) after each deposition (See more details in the experimental section).

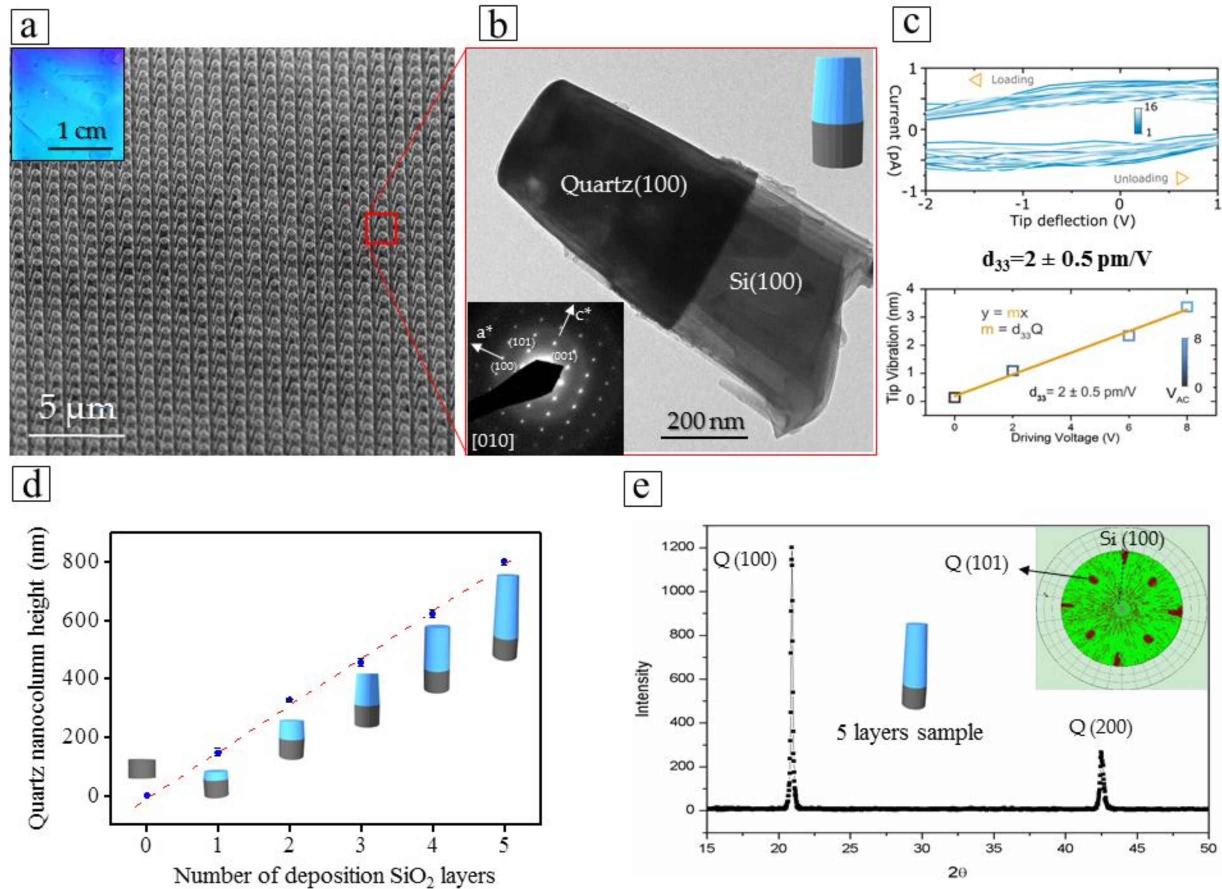

Fig. 2. **1D Lithographic patterning of epitaxial quartz thin films using LIL process.** **(a)** SEM image of anetwork of 600 nm thick epitaxial quartz nanocolumns. The inset image shows a low-resolution optical image of the sample. **(b)** Transmission Electron Microscopy image and electron diffraction measurement (inset image) of the α-quartz/Si interface of a single nanocolumn. **(c)** DPFM spectroscopic measurements on an 800 nm height quartz film obtained with a loading rate of 95000 µN/s. **(d)** Graphic that shows the control of quartz nanocolumns height with the number of multideposited silica sol gel layers before crystallization. **(e)** Long range θ-2θ XRD pattern with a perfect texture of the (100) α-quartz crystallographic phase after lithographic process. The inset image shows a pole figure of a 5-layer lithographed quartz film with (100) α-quartz[100]*‖(100) Si[100]* epitaxial relationship.

2.2. Soft nanoimprint lithography on Sr-SiO_2 sol-gel to nanostructurate epitaxial quartz films.

1
2
3
4
5
6
7
8
9
10
11
12
13
14
15
16
17
18
19
20
21
22
23
24
25
26
27
28
29
30
31
32
33
34
35
36
37
38
39
40
41
42
43
44
45
46
47
48
49
50
51
52
53
54
55
56
57
58
59
60

As an alternative route to LIL lithographic process, we applied soft Nano-Imprint Lithography (NIL), which combines top-down and bottom-up (sol-gel) approaches in order to produce epitaxial quartz nanopillar arrays on silicon with a precise control of pillar diameters and heights and inter-pillar distances. For this lithographic technique we first deposited a Sr-silica layer to promote the adhesion of a second layer which was printed with the PFMS mold. We want to emphasize that with this methodology we have reached unprecedented heights of 2 μm (see Figs. 3a and S5). The experimental procedure consisted in the combination of dip-coating process to synthetize Sr-silica xerogel films of controlled thicknesses on (100) silicon substrates with LIL and Nano-Imprint (NIL) lithographic techniques. In a first top-down fabrication step, large scale Si (100) masters made of nanopillars arrays were obtained by using LIL lithography and transferred by reactive ion etching at low pressure. Then, a second step involved preparing high quality PolyDiMethylSiloxane (PDMS) molds from Si(100) masters (see Fig. 3a) which we used to produce imprinted Sr-silica pillars with controlled diameter and height on silicon, as illustrated in figure 3b and figure S6.

1
2
3
4
5
6
7
8
9
10
11
12
13
14
15
16
17
18
19
20
21
22
23
24
25
26
27
28
29
30

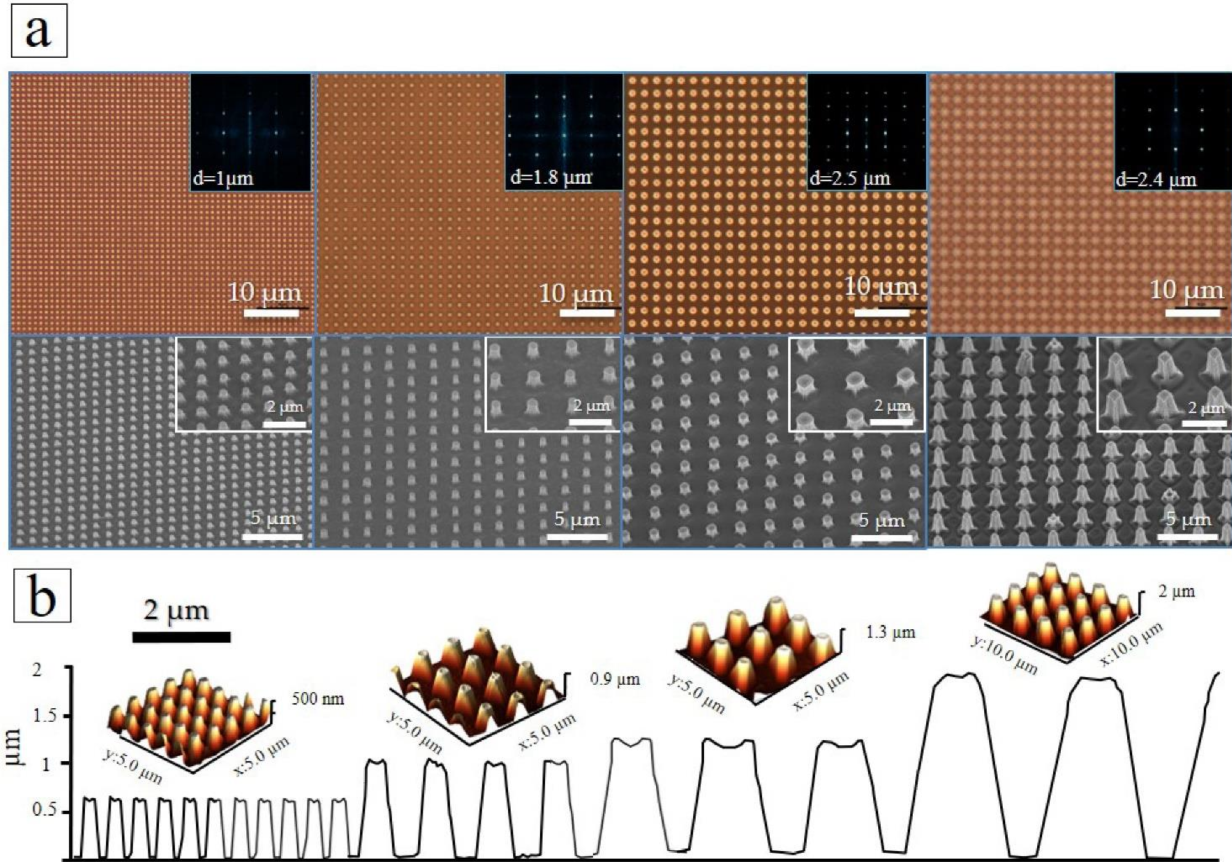

31
32
33
34
35
36
37
38

Fig. 3. (a) Optical images of Si (100) masters used along this work obtained by using LIL lithography. The inset images correspond to the 2D Fourier transform (FFT) which gives the separation distance between silicon columns i.e. 1, 1.8, 2.5 and 2.4 μm, respectively. FEG-SEM images (below) of printed Sr- silica nano-pillars with controlled diameters of 400, 650, 850 and 1000 nm on silicon. The inset pictures show FEG-SEM images of pillars at higher magnification. **(b)** 3D AFM images showing silica nanostructured films prepared by NIL lithography. Below you can distinguish the profile analysis of the AFM image, revealing a perfect transfer of the different features.

39
40
41
42
43
44
45
46
47
48
49
50
51
52
53
54
55
56
57
58
59
60

Finally, imprinted epitaxial (100) α-quartz nano-pillars arrays on silicon were obtained applying a thermal treatment at 1000ºC for 5 hours (see Fig. 4). Both optical microscope and SEM images shows Sr-silica xerogel nanopatterns composed of 600 nm height columns before crystallization process, see Fig. 4a. The crystallized sample is shown in Fig. 4b, which exhibits the characteristic quartz grain boundaries at the nanostructured surface film (see optical image in figure 4b). Atomic resolution high angle annular dark field (HAADF) image of a single quartz nanocolumn/silicon interface reveals the epitaxial growth of quartz layer with an atomically sharp interface with the

silicon substrate as shown in Fig. 4d (see also Figs. S7 in S.I.). In order to attain both a continuous nanostructured crystalline quartz film and a perfect nano-imprinted pattern, the dip coater deposition conditions have to be optimized. Likewise, a first mesoporous silica xerogel adhesion layer was needed to obtain an optimal print of PDMS molds on the Si(100) substrate (see Fig. 4c). This adhesion layer is consolidated at 450 °C during 5 min, before the deposition of the final printable silica layer. Both layers have the same thickness (200 nm) and are deposited under the same conditions i.e. at 25°C, 45% of humidity after applying a withdrawal speed of 300 mm min^{-1} with the dip-coater. It is worth noting that the withdrawal speed of 300 mm min^{-1} determines the thickness of the film[35] which, is indeed a critical factor to produce continuous nanostructured quartz layers. Below this critical withdrawal speed, the nucleation and crystallization of quartz layers is partial. As a result, fully crystallized films with a 100% surface coverage cannot be obtained for film thicknesses below 200 nm (see Fig. S8a). This trend is also reflected by the XRD patterns of the films which display higher intensities of the α-quartz (00L) reflections for increasing withdrawal speeds (see Fig. S8b)

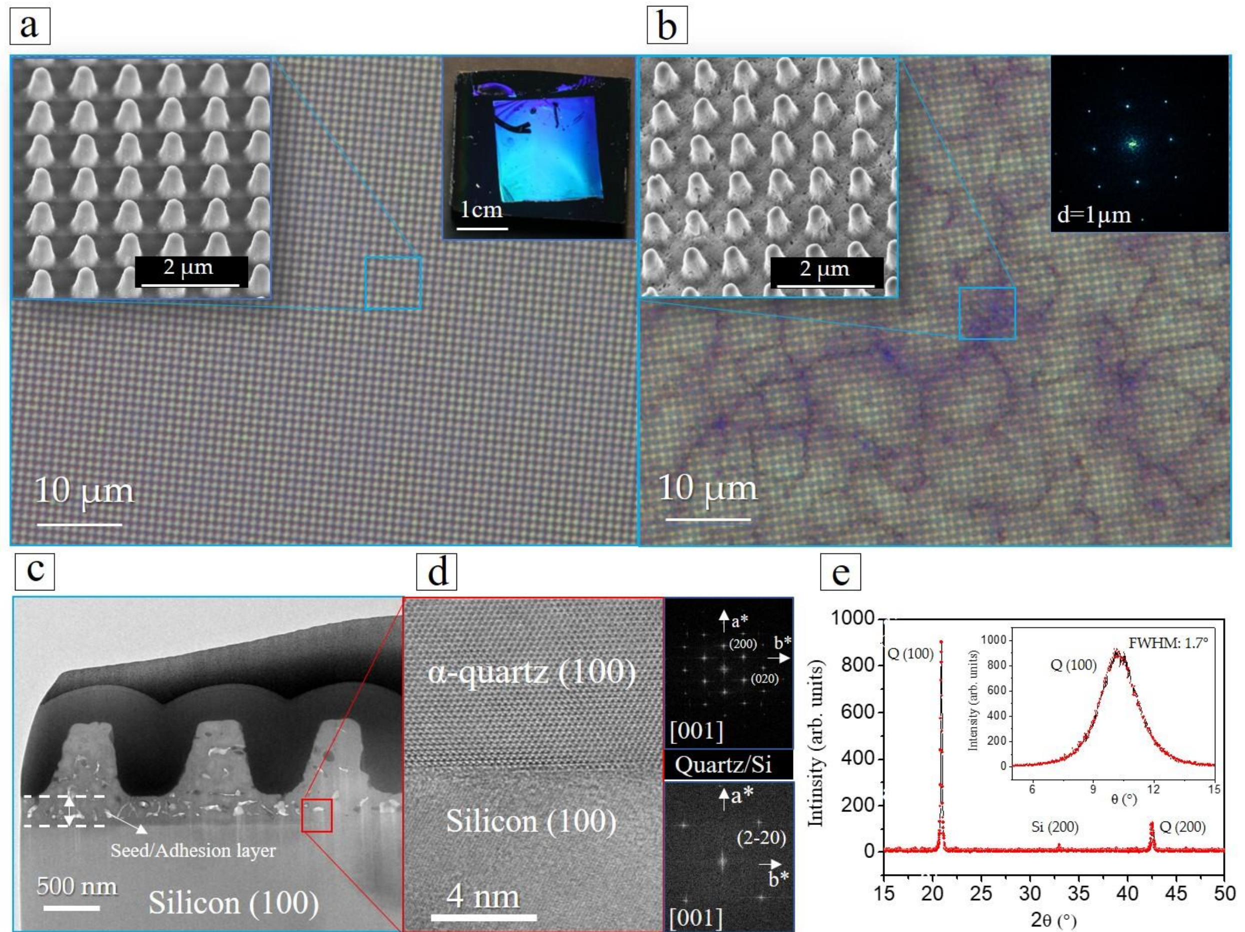

Fig. 4. Crystallization of Sr-silica xerogel nanopattern. **(a)** Optical image of Sr-silica xerogel nanopattern composed of 500 nm height columns performed by NIL lithographic process before crystallization process. The inset figures show a higher magnification FEG-SEM image illustrating the morphology of the Sr-silica xerogel nanopattern (left side) and an optical image that exhibits the light diffraction after interaction with the quartz nanocolumn pattern (right side). **(b)** Optical image of the Sr-silica xerogel nanopattern sample after crystallization. Notice that it is possible to observe the formation of typical quartz grain boundaries. The inset images show a higher magnification FEG-SEM image of the quartz nanopattern (left side) and the 2D-FFT of quartz columns that confirms the perfect replica by exhibiting the same spatial separation and dimensions than the corresponding silicon master i.e. 1 µm of separation and 1 µm of height. (right side). **(c)** Low magnification high angle annular dark field (HAADF) Z-contrast image of a quartz nanocolumn grown on the Si substrate assisted by the Sr^{2+} catalyst at 1000 °C, 5 hours. **(d)** Atomic resolution Z-contrast image of a single (100)-oriented quartz nanocolumn viewed along the [100]-crystallographic direction. Inset figures show the corresponding FFT of both the quartz film and the silicon substrate. **(e)** θ-2θ XRD pattern with a perfect texture of the (100) α-quartz crystallographic phase after lithographic process. The inset shows a rocking curve of the quartz (100) reflection with a full width at half maximum of 1.7°.

1
2
3
4
5
6
7
8
9
10
11
12
13
14
15
16
17
18
19
20
21
22
23
24
25
26
27
28
29
30
31
32
33
34
35
36
37
38
39
40
41
42
43
44
45
46
47
48
49
50
51
52
53
54
55
56
57
58
59
60

To evaluate the piezoelectricity of the nanoimprinted quartz columns we employed PFM. The obtained d_{33} value was of the same order of magnitude as those corresponding to the quartz films before lithographic process and the bulk material (see Fig. 5). The PFM amplitude image is represented in Figure 5a and the inset shows the topographic AFM image of crystallized nanocolumns. Notice that the areas surrounding the nanocolumns show a slight change in the PFM amplitude, the signal remains constant at the top of the columnar structures and at the quartz film surrounding the base of these pillars. The change of the PFM amplitude signal in the perimeter of the nanocolumns is attributed to a topographic crosstalk artifact which is well known and reported by the community[36]. We were able to corroborate the electromechanical behavior of our films by performing point-out spectroscopy measurements, see Fig. 5b. The electromechanical behavior of the structures was studied using frequency-sweeps to display the PFM contact resonant circuit. The electromechanical behavior is studied outside and inside of the nanocolumns by placing the AFM tip in each respective position. The data shows an increase of resonant amplitude with an increase of the applied AC bias, in a similar way as depicted in Fig. 2c, confirming that the nanostructuration has not been detrimental to the electromechanical properties.

Likewise, this nanostructuration methodology of epitaxial quartz thin films on silicon by NIL lithography is general for several kinds of patterns including lines as those shown in Fig. S9.

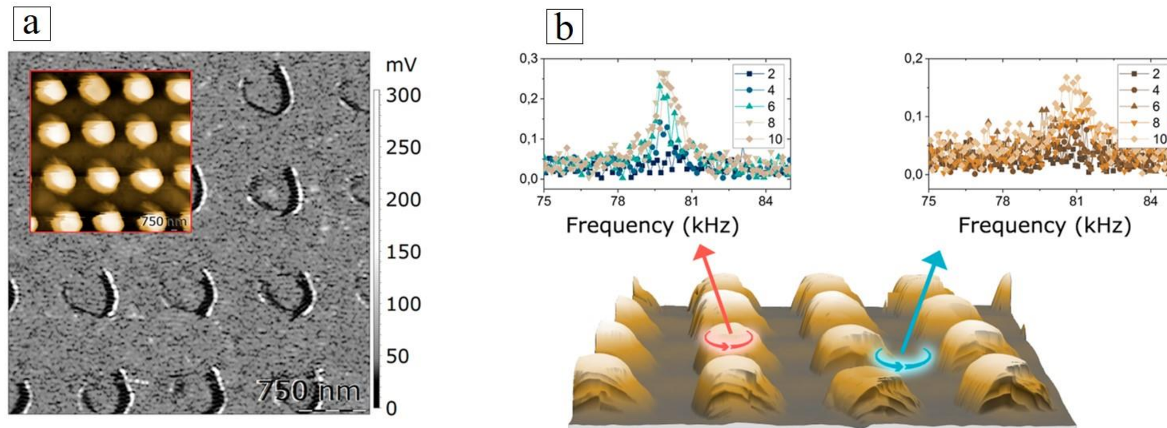

Fig 5. Piezoelectric response of epitaxial nanostructured quartz films using NIL lithographic process. (a) PFM amplitude and topography (inset) recorded simultaneously while applying a tip-substrate AC voltage of 10 V, showing area similar tip vibration level at the background film and top nanostructures. Point-out spectroscopy measurements recorded on top of the structures and bottom film, for different applied AC bias. **(b)** The data shows an increase of the PFM resonant frequency amplitude with an increase of the applied AC bias, confirming our expectation that piezoelectric functionality is preserved.

2.3. Self-assembled $SrCO_3$ nanoparticles as nanomasks for lithographic patterning of epitaxial quartz thin films on silicon.

Films with a Sr/SiO_2 molar ratio of 0.05 exhibit an outcropping of $SrCO_3$ nanoparticles at the surface, driven by a chemical reaction between SrO, CO_2 and H_2O, have been shown elsewhere[37]. These observations revealed the assembly of sintered $SrCO_3$ nanoparticles during the annealing treatment at 1000°C, whereas now, as illustrated in Fig. 6, we exploit these $SrCO_3$ nanoparticles as nanomasks to produce an array of quartz nanopillars from films. Indeed, solid $SrCO_3$ nanoparticles are extremely stable under the reacting ion etching conditions. By this simple approach, illustrated in Fig. 1 and Fig. 6, one can produce arrays of quartz nanopillars having diameters down to 60 nm and a maximum height of 400 nm, depending on the original quartz film thickness. This type of behavior has been reported for CaF_2 nanoparticles formed after a chemical reaction with the plasma etching[38]. In that case, the chemical transformation of the $Ca_xTi_{(1-x)}O_{(2-x)}$ present within the

amorphous silica layer into the homogeneous dispersions of CaF_2 nanoparticles, was used as a particulate nanostencil system to produce an array of silicon nanopillars[38]. In our case, the $SrCO_3$ nanoparticles are formed during quartz crystallization and remained extremely stable during the RIE etching process, acting as an efficient nanomask that protects quartz from the plasma etching. This feature can be observed in Figure 6 that shows $SrCO_3$ nanoparticles before and after RIE process. Figure 6a and S10 show the typical morphology and size of the $SrCO_3$ nanoparticles on top of the epitaxial quartz thin film.

The efficacy of the process was investigated by electron microscopy and electron diffraction characterization was used to assess the crystalline structure of the quartz nanopillars (see figure 6). The etching has been applied in 100W RF and 200W LF of an inductively coupled plasma reactive ion etching (ICP-RIE) reactor using CHF_3/O_2 gas mixture (see more details in experimental section). The electron diffraction pattern of a single quartz nanopillar presented in Fig. 6b reveals perfect quartz crystallinity similar to that of the initial quartz film.

The morphology of the motifs is conical rather than needle-like as a result of an isotropic etching of CHF_3/O_2 flux. With the aim of producing networks of needle-like quartz nanostructures, we used ionized gases and gas mixtures such as Ar, CHF3, SF6 in order to control the anisotropy of the etching[39]. Unfortunately, under these etching conditions, quartz thin film and $SrCO_3$ nanoparticles were totally destroyed after 4 min (see figure SI 11).

1
2
3
4
5
6
7
8
9
10
11
12
13
14
15
16
17
18
19
20
21
22
23
24
25
26
27
28
29
30
31
32
33
34
35
36
37
38
39
40
41
42
43
44
45
46
47
48
49
50
51
52
53
54
55
56
57
58
59
60

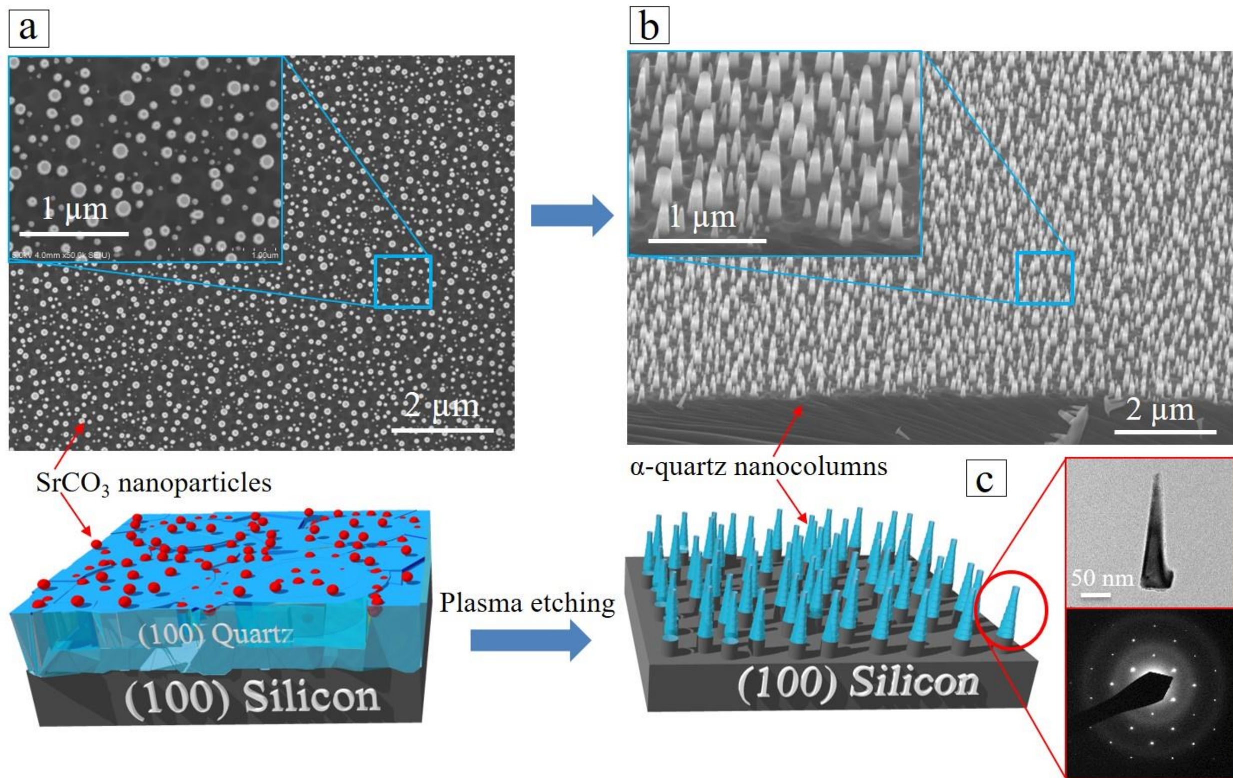

Fig. 6. $SrCO_3$ nanoparticles as nanomasks to produce an array of quartz nanopillars. (a) FEG-SEM image illustrating the morphology of sintered $SrCO_3$ nanoparticles at 1000°C. The inset image shows a picture with a higher magnification. **(b)** FEG-SEM image illustrating the morphology of quartz single crystal conical-like nanopillars after RIE etching of a film. The inset image shows a small picture **b** with a higher magnification. General schematic of RIE etching to produce first nano lithographic patterns on epitaxial quartz thin films. **(c)** Electron diffraction pattern of a conical-like nanopillar in c shows a perfect crystallinity after the nanomask lithographic process.

3. Conclusion

The combination of top-down and bottom-up methodologies enabled the nanostructuration of piezoelectric quartz films, epitaxially grown on (100)-silicon substrates. We have used scalable lithographic methodologies that do not require masks to generate highly ordered 1D quartz patterns consisting of vertical quartz nanocolumns with diameters and heights ranging from 50 nm to 800 nm and heights ranging from 200 nm to 2 µm. The nanostructuration engineering of epitaxial quartz films on silicon presented here is general for several kind of patterns and has being produced by

only using exclusively lithographic methodologies. LIL lithographic allowed preparing quartz columns with diameters between 400 and 800 nm and heights in the range of 200 nm to 1000 nm, thanks to a novel multilayer film process consisting in the sequential deposition and consolidation of several gel layers. With this combination of methodologies, epitaxial 1D-quartz nanostructures maintain the crystallinity and epitaxial orientation of (100) α-quartz[100]* ‖ (100) Si[100]*. On the other hand, we have established the conditions to replicate Sr-silica pillars from different PDMS molds by the combination of NIL and sol gel. Specifically, using a withdrawal speed of 300 mm min^{-1} at 25°C and 45% of humidity and the deposition of adhesion layer it is possible to obtain a perfect nano-imprinted crystalline continuous quartz pattern. Thus, the interplay between temperature, humidity, dip-coating conditions, and epitaxial growth plays a key role for the fabrication epitaxial quartz nanopillars on silicon substrates by NIL lithography. Finally, the controlled outcropping of $SrCO_3$ nanoparticles on top of epitaxial quartz thin films, which play the role of a nanomask under the reactive ion etching process, allows obtaining quartz nanopillars with diameters down to 60 nm and a maximum height of 400 nm. In all cases, the patterning of quartz films preserves their piezoelectric properties. We used PFM technique, (in standard converse piezoelectric mode and in the direct piezoelectric mode named DPFM), to quantify the piezoelectric coefficient d_{33} of nanostructured quartz films.

This work validates the complementarity between soft-chemistry and top-down lithographic techniques for the patterning of epitaxial quartz thin films integrated on silicon. As a result, the control at the nanoscale over the shape, micro- and nano-patterning of quartz thin films opens up the opportunity to engineer novel micro and nanoelectromechanical quartz systems for high frequency and sensor applications.

4. Experimental Section

4.1.Synthesis

Solution preparation: All the chemicals were purchased from Sigma-Aldrich and used without any further purification. In a typical process, we first prepared a solution (solution A) by adding 0.7 g Brij-58 into 23.26 g absolute ethanol, then 1.5 g HCl (37%), 4.22 g tetraethyl orthosilicate (TEOS) and stirring the solution during 16 hours. Notice that the solution A can be stirred for a period of time (4-18 hours) before its ageing. After that, a 1 M aqueous solution of Sr^{2+} was prepared with $SrCl_2{\cdot}6H_20$ (Solution B). The solution used to prepare mesoporous Sr- silica films by dip-coating (Solution C) was obtained by adding 275 μL Solution B into 10 mL of as-prepared Solution A and stirring it for 10 min. The films were always obtained not later than 40 min after preparing solution C, as Sr^{2+} is not stable. The amount of Sr introduced with Solution B is such a that in solution C the Sr/SiO_2 molar ratio is 0.05 and the final molar composition TEOS:Brij-58:HCl:EtOH:$SrCl_2$=1:0.3:0.7:25:0.05.

Gel films by dip-coating: layer gel films on Si (100) substrates were prepared with a ND-DC300 dip-coater (Nadetech Innovations) equipped with an EBC10 Miniclima Device to control the surrounding temperature and relative humidity. During the dip-coating, we fixed the ambient temperature and relative humidity as 25ºC and 40% and the thickness of film was controlled by the withdrawal rate. In this study, all the films were made with a withdrawal rate of 5 mm/s to ensure the perfect crystallization and nanoimprint process. After dip-coating, as-prepared gel films were consolidated with a thermal treatment during 5 min at 450 ºC under air atmosphere. In order to obtain thicker films, and therefore taller nanocolumns, multi-layer gel films were obtained by repeating the required number of times the process of mono-layer preparation on the same substrate.

Crystallization: As-prepared gel films were introduced into a furnace already at 1000ºC in air atmosphere and held at this temperature for 300 min. The crystallized films were recovered after cooling of the furnace to room temperature.

1
2
3
4
5
6
7
8
9
10
11
12
13
14
15
16
17
18
19
20
21
22
23
24
25
26
27
28
29
30
31
32
33
34
35
36
37
38
39
40
41
42
43
44
45
46
47
48
49
50
51
52
53
54
55
56
57
58
59
60

4.2.Structural Characterization and Piezoelectric Measurements

X-Ray Diffraction (XRD): The crystalline textures and rocking curve measurements of films were performed on a on a D8 discovery Bruker diffractometer equipped with a EIGER2 R 500K detector (3 s acquisition each 0.02º in Bragg-Brentano geometry, with a radiation wavelength of 0.154056 nm). Epitaxial relationship was analyzed through X-ray diffraction measurements by using a Bruker AXS GADDS equipped with a 2D X-ray detector. *Optical Microscopy*: The optical images of films were obtained in an Olympus BX51M optical microscope equipped with a Nikon DS-Fi3 camera. *Field Emission Gun Scanning Electron Microscopy (FEG-SEM)*: The microstructures of the films were investigated with a FEG-SEM model Su-70 Hitachi, equipped with an EDX detector X-max 50 mm^2 from Oxford instruments. *Transmission Electron Microscopy (TEM)*: Cross-sectional studies of films were performed by using a FEI Titan3 operated at 80 kV and equipped with a superTwin® objective lens and a CETCOR Cs-objective corrector from CEOS Company. Electron diffraction studies were performed in a JEOL 1210 operated at 120 kV. *Atomic Force Microscopy (AFM)*: The topography of nanostructured quartz films was studied by AFM in a Park Systems NX-Scanning Probe Microscopy (SPM) unit. Piezoelectric characterization through the direct piezoelectric effect was made by Direct Piezoelectric Force Microscopy[33] in an Agilent 5500LS instrument using a low leakage amplifier (Analog Devices ADA4530) with Platinum solid tips (Rockymountain Nanotechnology RMN-25 PtIr200H). PFM measurements were performed in an Agilent 5500LS using a long-tip shank length tip[40] to diminish electrostatic interaction (RMN 25PtIr300b) while working in the resonant frequency (~ 80 kHz). A Periodically Poled Lithium Niobate sample from Bruker AFM was used as a reference testing platform.

4.3.Quartz thin films nanostructuration

1
2
3
4
5
6
7
8
9
10
11
12
13
14
15
16
17
18
19
20
21
22
23
24
25
26
27
28
29
30
31
32
33
34
35
36
37
38
39
40
41
42
43
44
45
46
47
48
49
50
51
52
53
54
55
56
57
58
59
60

Optical lithography. First set of samples has been fabricated by top-down approach using conventional optical photolithography following by anisotropic plasma etching. First, linear micrometer scale patterns have been insolated in 1.1 µm thick photoresist layer (ECI from MicroChemicals) using a conventional mask aligner (SUSS Mask Aligner MA 6). The patterns were transferred on epitaxial quartz thin films (see figure S1) by performing plasma etching using fluoroform chemistry, low pressure (5 mTorr), and 100 W bias power in pure capacitive coupling plasma (CCP). Finally, the remaining ECI resist was exposed in acetone and rinsed in isopropanol.

Laser interferential lithography (LIL)

In order to produce an epitaxial quartz nanocolumn pattern from films, we used a positive photoresist, AZ MIR 701, which was exposed using the interferential lithography technique to obtain a network of dots after the using a developer, AZ726. This procedure allows to rapidly obtain periodic design over a large surface (~cm^2) without the need of a lithographic mask[13]. For the quartz pattern in Figure 2, a 405 nm wavelength laser with a divergent beam was reflected by two mirrors shifted with an angle of 10° which resulted in an interferometric pattern with a pitch of 1 µm. To obtain the dot pattern two exposures were needed, a first exposure created periodic lines and a second exposure shifted by 90° with respect to the first exposure generated perpendicular periodic lines. The result of these two exposures, after development, generates the dots. Finally, the samples were anisotropically etched by inductively coupled plasma reactive ion etching (ICP-RIE) (model Corial 210IL ICP-RIE etch system) using CHF_3/O_2 gas mixture. RIE conditions for etching of the sample and then produce a periodic pattern of quartz pillars of 1 µm depth were the following: power:120W RF, 400 W LF, gas: CHF_3 100 sccm-O_2 20 sccm (standard cubic centimeter per minutes), pressure: 10 mTorr and time: 10 min. ICP-RIE produces a dry and directional etching induced by a mixture of CHF_3 and O_2 plasma.

Soft nano-imprint lithography (NIL) Preparation

1
2
3
4
5
6
7
8
9
10
11
12
13
14
15
16
17
18
19
20
21
22
23
24
25
26
27
28
29
30
31
32
33
34
35
36
37
38
39
40
41
42
43
44
45
46
47
48
49
50
51
52
53
54
55
56
57
58
59
60

Moulds preparation: Si masters were elaborated with different structures and heights using LIL lithography. PDMS (polydimethylsiloxane) reactants (90 w% RTV141A; 10 w% RTV141B from BLUESIL) were transferred onto the master and dried at 70 °C for 1 h before unmoulding.

Then, a first silica layer seed was deposited at a constant relative humidity of 45% with controlled withdrawal speeds of 5 mm/s in order to adjust the final thickness to 200 nm, and was consolidated at 450ºC for 10 min. Importantly, this layer has two different functionalities: (i) as a seed layer to produce a continuous and homogeneous epitaxial quartz thin film on silicon and (ii) as an adhesion layer to faultlessly replicate the columnar shape from the PDMS mould. Then, a new layer of the same solution was deposited under the same conditions for printing. Notice that the Surfactant Brij-58 included in the final sol-gel Solution C did not change the wetting properties of the sol.

After the last dip-coating, the substrates were quickly introduced during 1 min into a custom-designed chamber under a controlled temperature of 25 °C using and a constant humidity of 45%. Imprinting of sol–gel films with a PDMS mould involves the following steps. First, moulds were degassed under vacuum (10 mbar) for 20 min before direct application on the as-prepared xerogel films kept in a controlled environment, without additional pressure. After 1 min, the samples were transferred to a 70 °C stove for 2 min and then to a 120 °C for 2 min to consolidate the xerogel films before peeling off the PDMS mould. Next, the sol–gel replicas were annealed at 450 °C for 10 min for consolidation. Finally, sample was crystallized in to quartz at 1000ºC for 5h in air atmosphere.

Nanomasks lithography

Quartz samples covered by $SrCO_3$ nanomasks were anisotropically etched by inductively coupled plasma reactive ion etching (ICP-RIE) (model Corial 210IL ICP-RIE etch system) using CHF_3/O_2 gas mixture. The RIE conditions to engrave the sample and then produce quartz nanopillars pattern

1
2
3 of 300 nm depth were the following: power:120W RF, 400 W LF, gas: CHF_3 100 sccm-O_2 20 sccm,
4
5 flux: pressure: 10 mTorr and time: 10 min.
6
7
8 Isotropic etching conditions used in samples of Fig. S10 were the following: power: 100W RF, 200
9
10 W LF, gas: CHF_3 80 sccm-O_2 10 sccm, SF6 20 sccm, pressure: 10 mtorr and time: 4 min (for a 300
11
12 nm thick quartz layer).
13
14
15 Notice that if requested the $SrCO_3$ nanoparticles can be dissolved by dipping the sample into a
16
17 nitric acid solution (3 M) for 2 hours after quartz crystallization[37].
18
19
20
21
22 **TOC FIGURE**
23

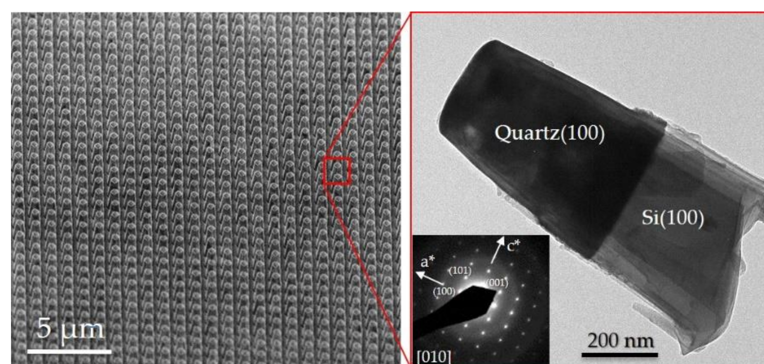

24
25
26
27
28
29
30
31
32
33
34
35
36
37 **Supporting Information.** Brief statement in non-sentence format listing the contents of the
38 material and additional data about the microstructural and physical characterization of patterned
39 quartz films supplied as Supporting Information.
40
41
42 **Acknowledgements**
43

44 This project has received funding from the European Research Council (ERC) under the European
45 Union's Horizon 2020 research and innovation programme (No.803004); the French Agence
46
47 Nationale pour la Recherche (ANR), project Q-NOSS ANR ANR-16-CE09-0006-01; the Spanish
48 Ministry of Science Innovation and Universities in co-funding with European Social funds through
49 the Severo Ochoa Program for Centers of Excellence in R&D (SEV-2015-0496) and the Ramón y
50
51 Cajal program (J.G., RyC-2012-11709); the Generalitat de Catalunya (2017SGR00765). Q.Z. was
52 financially supported by China Scholarship Council (CSC) with No.201506060170. Q.Z.'s work
53 was done as a part of the Ph.D program in Materials Science at Universitat Autònoma de Barcelona.
54
55 The authors thank the "Laboratorio de Microscopías Avanzadas-Instituto de Nanociencia de
56 Aragón" for offering their expertise in the preparation of TEM cross-sections. A. Crespi from
57
58
59
60

1
2
3
4
5
6
7
8
9
10
11
12
13
14
15
16
17
18
19
20
21
22
23
24
25
26
27
28
29
30
31
32
33
34
35
36
37
38
39
40
41
42
43
44
45
46
47
48
49
50
51
52
53
54
55
56
57
58
59
60

XRD diffraction service is acknowledged for pole figure measurements. FEGSEM instrumentation was facilitated by the Institut des Matériaux de Paris Centre (IMPC FR2482) and was funded by Sorbonne Université,CNRS and by the C'Nano projects of the Région Ile-de-France. We thank David Montero for performing the FEGSEM images.

References

1. Vila-Fungueiriño JM, Bachelet R, Saint-Girons G, et al. Integration of functional complex oxide nanomaterials on silicon. Frontiers in Physics. 2015;3.
2. Craighead HG. Nanoelectromechanical Systems. Science. 2000;290: 1532-1535.
3. Ramesh R, Schlom DG. Orienting Ferroelectric Films. Science. 2002;296: 1975-1976.
4. Warusawithana MP, Cen C, Sleasman CR, et al. A Ferroelectric Oxide Made Directly on Silicon. Science. 2009;324: 367-370.
5. Bottom VE. Introduction to quartz crystal unit design (Van Nostrand Reinhold electrical/computer science and engineering series). New York: Van Nostrand Reinhold, 1982.
6. Benes E, Gröschl M, Burger W, Schmid M. Sensors based on piezoelectric resonators. Sensors and Actuators A: Physical. 1995;48: 1-21.
7. Sauerbrey G. Verwendung Von Schwingquarzen Zur Wagung Dunner Schichten Und Zur Mikrowagung. 1959.
8. Galliou S, Goryachev M, Abbe P, Vacheret X, Tobar M, Bourquin R. Quality Factor Measurements of Various Types of Quartz Crystal Resonators Operating Near 4 K. 2015.
9. Danel JS, Delapierre G. Quartz: a material for microdevices. Journal of Micromechanics and Microengineering. 1991;1: 187.
10. Imbert B, Reinhardt A, Ricart T, et al. Thin film quartz layer reported on silicon. 2011 Joint Conference of the IEEE International Frequency Control and the European Frequency and Time Forum (FCS) Proceedings, 2011:1-4.
11. Kamijo A, Monoe S, Murayama N, Saito T, Kimura N. Wafer-level quartz dry etching technology. 2014 IEEE International Frequency Control Symposium (FCS), 2014:1-4.
12. Chapellier P, Lavenus P, Bourgeteau-Verlhac B, Gageant C, Traon OL, Dulmet B. Aspect ratio dependent etching in advanced deep reactive ion etching of quartz. 2017 Symposium on Design, Test, Integration and Packaging of MEMS/MOEMS (DTIP), 2017:1-6.
13. Santybayeva Z, Meghit A, Desgarceaux R, et al. Fabrication of quartz microcylinders by laser interference lithography for angular optical tweezers: SPIE, 2016:5.
14. Young-Ik Sohn RM, Vivek Venkataraman, Marko Lončar. Mechanical and optical nanodevices in single-crystal quartz. arXiv.org > cond-mat >. 2017.
15. Sohn Y-I, Miller R, Venkataraman V, Lončar M. Mechanical and optical nanodevices in single-crystal quartz. Applied Physics Letters. 2017;111: 263103.
16. Lu H, Sadani B, Courjal N, et al. Enhanced electro-optical lithium niobate photonic crystal wire waveguide on a smart-cut thin film. Optics Express. 2012;20: 2974-2981.
17. Carretero-Genevrier A, Gich M, Picas L, et al. Soft-Chemistry-Based Routes to Epitaxial alpha-Quartz Thin Films with Tunable Textures. Science. 2013;340: 827-831.
18. Au - Carretero-Genevrier A, Au - Gich M. Preparation of Macroporous Epitaxial Quartz Films on Silicon by Chemical Solution Deposition. JoVE. 2015: e53543.
19. Zhang Q, Sánchez-Fuentes D, Gómez A, et al. Tailoring the crystal growth of quartz on silicon for patterning epitaxial piezoelectric films. Nanoscale Advances. 2019;1: 3741-3752.
20. Brinker CJ, Clem PG. Quartz on Silicon. Science. 2013;340: 818-819.

1
2
3
4
5
6
7
8
9
10
11
12
13
14
15
16
17
18
19
20
21
22
23
24
25
26
27
28
29
30
31
32
33
34
35
36
37
38
39
40
41
42
43
44
45
46
47
48
49
50
51
52
53
54
55
56
57
58
59
60

21. Mina IG, Kim H, Kim I, et al. High frequency piezoelectric MEMS ultrasound transducers. IEEE Transactions on Ultrasonics, Ferroelectrics, and Frequency Control. 2007;54: 2422-2430.
22. Hoffman-Kim D, Mitchel JA, Bellamkonda RV. Topography, Cell Response, and Nerve Regeneration. Annual Review of Biomedical Engineering. 2010;12: 203-231.
23. Martínez-Martín D, Fläschner G, Gaub B, et al. Inertial picobalance reveals fast mass fluctuations in mammalian cells. Nature. 2017;550: 500-505.
24. Sansen T, Sanchez-Fuentes D, Rathar R, et al. Nanoscale topography templates the organization of stable clathrin/AP-2 structures. bioRxiv. 2019: 767590.
25. Nikkhah M, Edalat F, Manoucheri S, Khademhosseini A. Engineering microscale topographies to control the cell–substrate interface. Biomaterials. 2012;33: 5230-5246.
26. Wang Y, Guo L. Nanomaterial-Enabled Neural Stimulation. Frontiers in Neuroscience. 2016;10.
27. Nurioglu AG, Esteves ACC, de With G. Non-toxic, non-biocide-release antifouling coatings based on molecular structure design for marine applications. Journal of Materials Chemistry B. 2015;3: 6547-6570.
28. Seo J-H, Park J, Kim S-I, et al. Nanopatterning by Laser Interference Lithography: Applications to Optical Devices, 2015.
29. Hamouda F, Bryche J-F, Aassime A, et al. Soft nanoimprint lithography on SiO2 sol-gel to elaborate sensitive substrates for SERS detection. AIP Advances. 2017;7: 125125.
30. Newnham RE. in Properties of materials: Anisotropy, Symmetry, Structure (Oxford University Press. 2005.
31. Abdollahi A, Domingo N, Arias I, Catalan G. Converse flexoelectricity yields large piezoresponse force microscopy signals in non-piezoelectric materials. Nature Communications. 2019;10: 1266.
32. Lew Yan Voon LC, Willatzen M, Wang Z-L. Model Calculation of the Piezoelectric Coefficient of Hexagonal 2D Materials. Advanced Theory and Simulations. 2019;2: 1800186.
33. Gomez A, Gich M, Carretero-Genevrier A, Puig T, Obradors X. Piezo-generated charge mapping revealed through direct piezoelectric force microscopy. Nature Communications. 2017;8: 1113.
34. Grosso D. How to exploit the full potential of the dip-coating process to better control film formation. Journal of Materials Chemistry. 2011;21: 17033-17038.
35. Faustini M, Louis B, Albouy PA, Kuemmel M, Grosso D. Preparation of Sol−Gel Films by Dip-Coating in Extreme Conditions. The Journal of Physical Chemistry C. 2010;114: 7637-7645.
36. Seol D, Kim B, Kim Y. Non-piezoelectric effects in piezoresponse force microscopy. Current Applied Physics. 2017;17: 661-674.
37. Drisko GL, Carretero-Genevrier A, Gich M, et al. Water-Induced Phase Separation Forming Macrostructured Epitaxial Quartz Films on Silicon. Advanced Functional Materials. 2014;24: 5494-5502.
38. Faustini M, Drisko G, Letailleur A, et al. Self-assembled Titanium Calcium Oxide Nanopatterns as versatile Reactive Nanomasks for Dry Etching Lithographic Transfer with High Selectivity. 2012.
39. Li L, Abe T, Esashi M. Smooth surface glass etching by deep reactive ion etching with SF6 and Xe gases. Journal of Vacuum Science & Technology B. 2003;21: 2545-2549.
40. Gomez A, Puig T, Obradors X. Diminish electrostatic in piezoresponse force microscopy through longer or ultra-stiff tips. Applied Surface Science. 2018;439: 577-582.

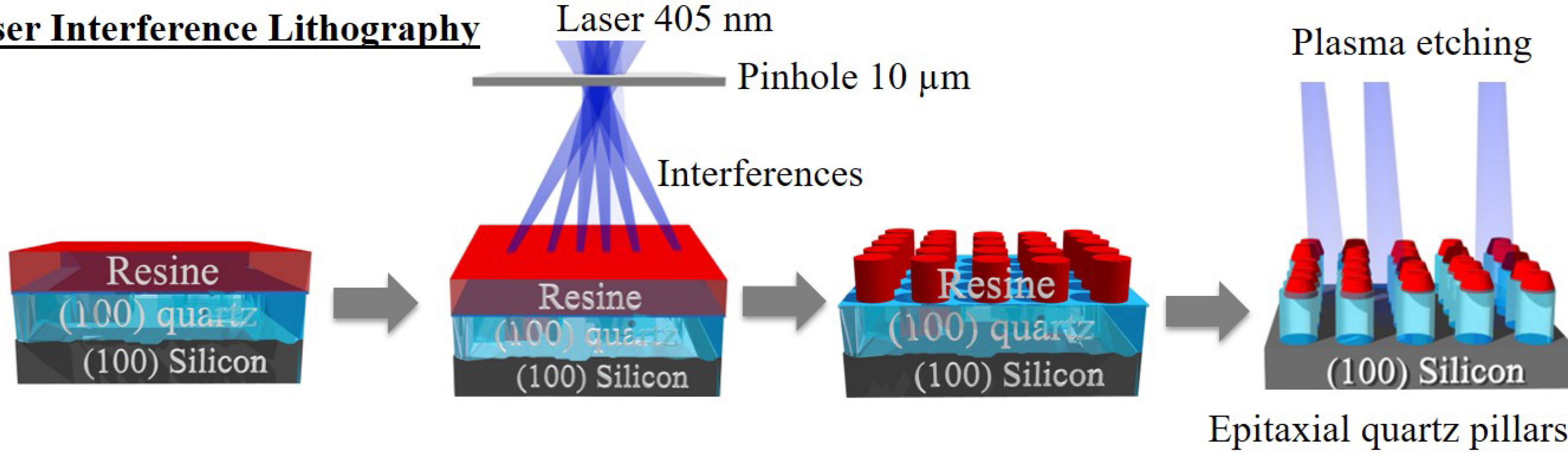
500 nm
Laser Interference Lithography
Laser 405 nm
Pinhole 10 µm
Interferences
Plasma etching
Resine
(100) quartz
(100) Silicon
Epitaxial quartz pillars

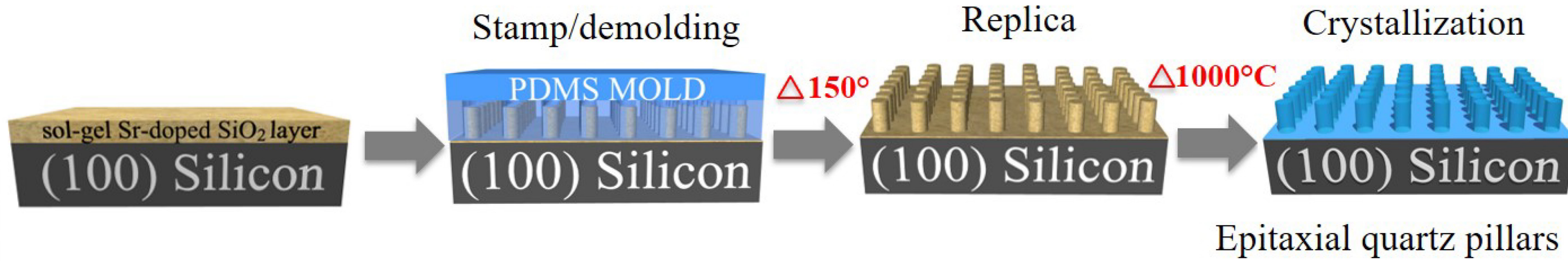
300 nm
Soft nanoimprint lithography
Stamp/demolding
Replica
Crystallization
sol-gel Sr-doped SiO₂ layer
PDMS MOLD
△150°
△1000°C
(100) Silicon
Epitaxial quartz pillars

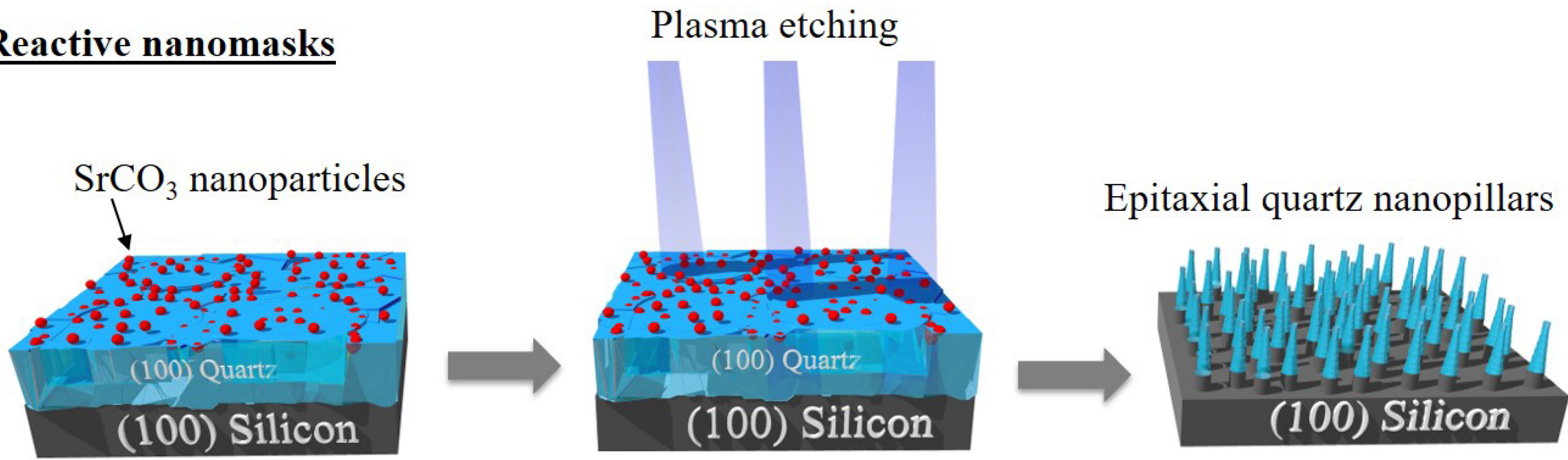
50 nm
Reactive nanomasks
Plasma etching
SrCO₃ nanoparticles
Epitaxial quartz nanopillars
(100) Quartz
(100) Silicon

a
1 cm
5 μm

b
Quartz(100)
Si(100)
a*
c*
(101)
(100)
(001)
[010]
200 nm

c
Tip Vibration (nm)
Frequency (kHz)
V_{AC}
d_{33}=2 ± 0.5 pm/V
y = mx
m = d_{33}Q
d_{33}= 2 ± 0.5 pm/V
Driving Voltage (V)

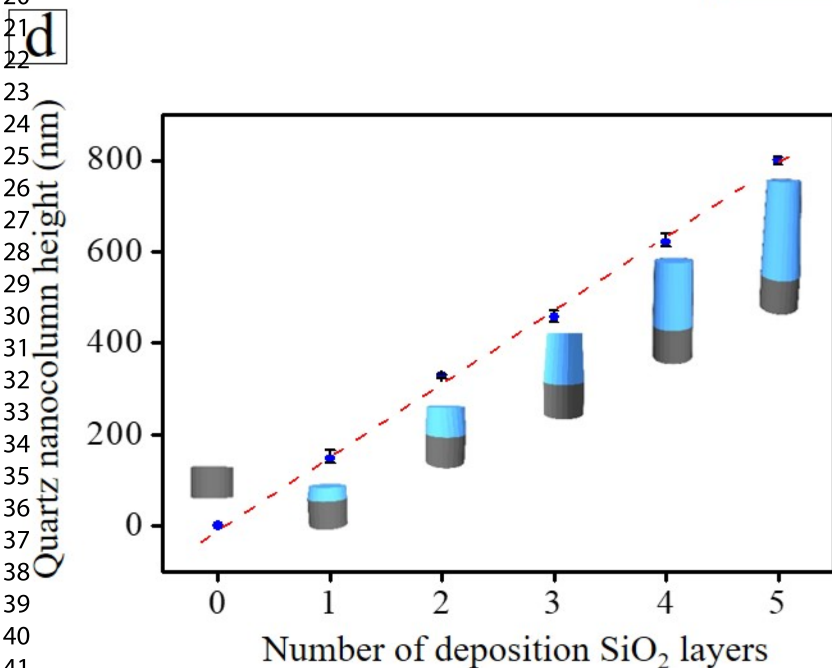

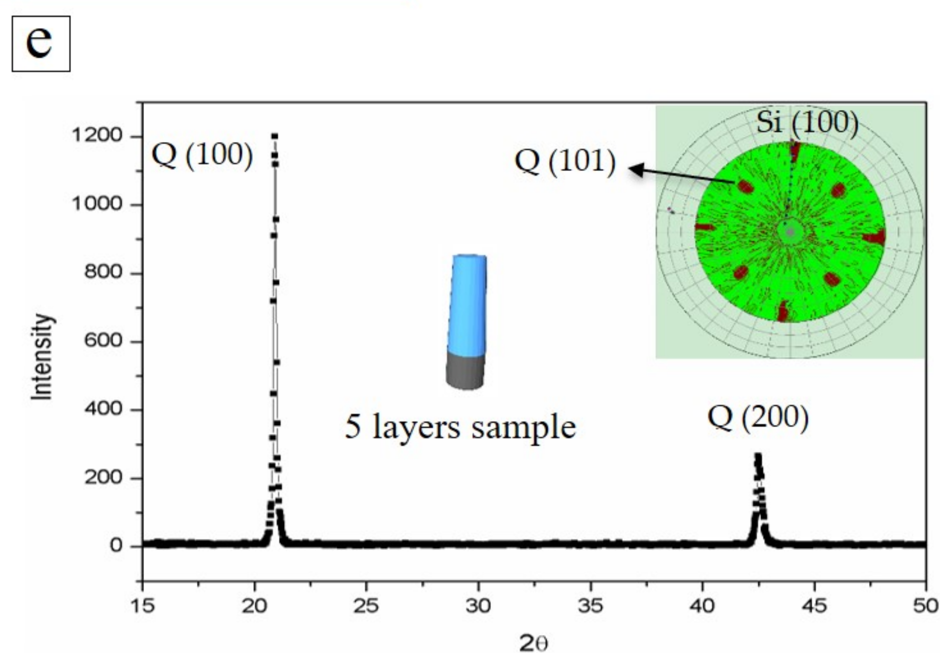

a

d=1μm
10 μm
d=1.8 μm
10 μm
d=2.5 μm
10 μm
d=2.4 μm
10 μm
2 μm
5 μm
2 μm
5 μm
2 μm
5 μm
2 μm
5 μm

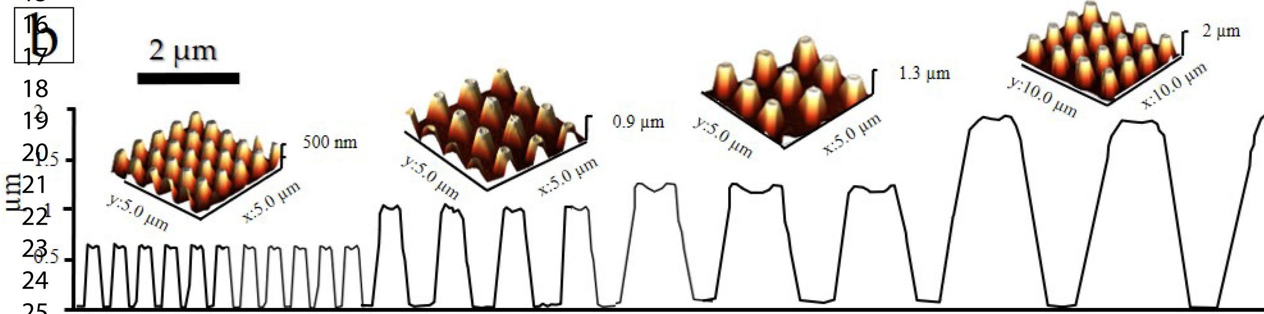

1
2
3
4
5
6
7
8
9
10
11
12
13
14
15
16
17
18
19
20
21
22
23
24
25
26
27
28
29
30
31
32
33
34
35
36
37
38
39
40
41

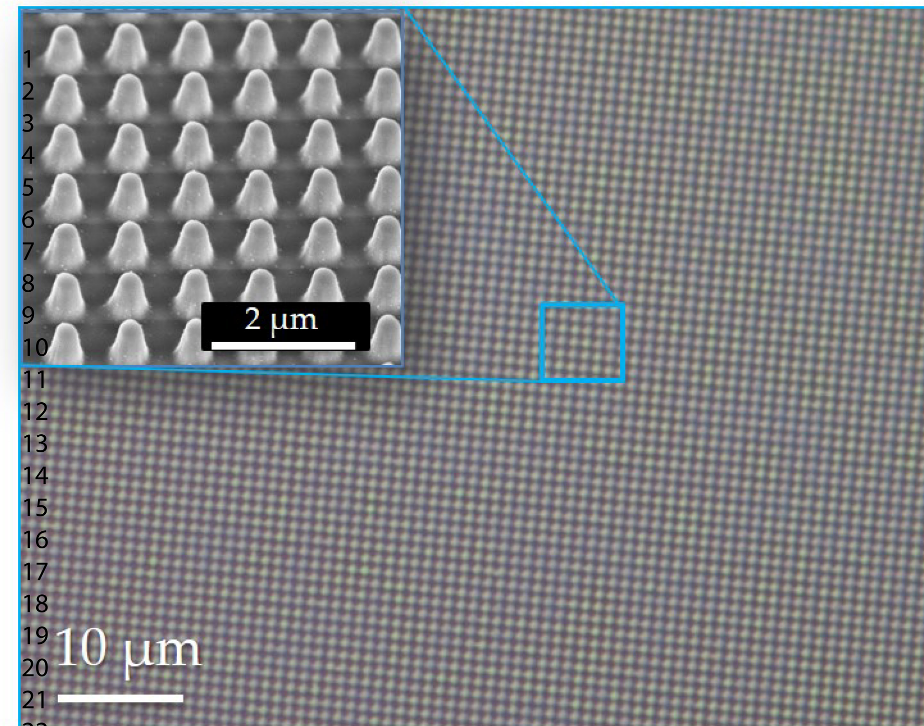

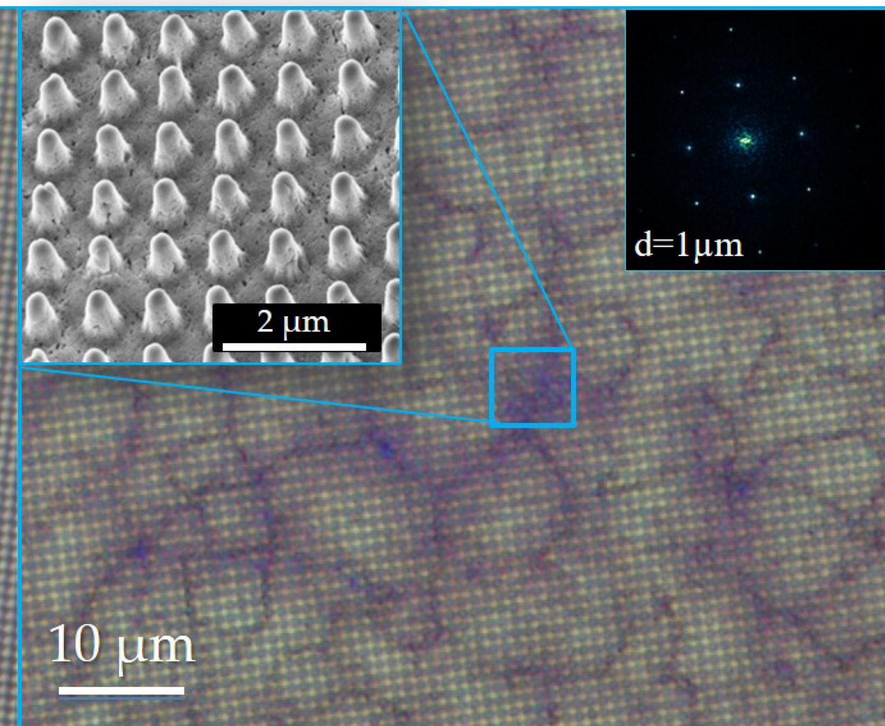

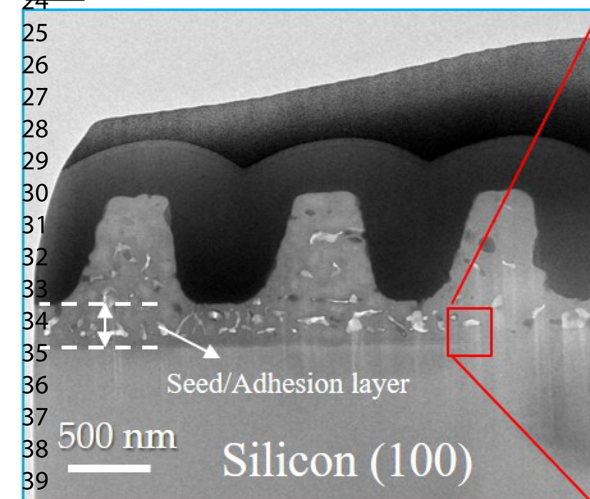

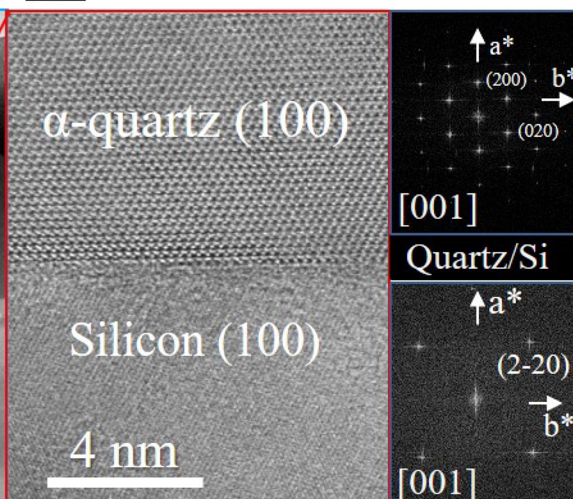

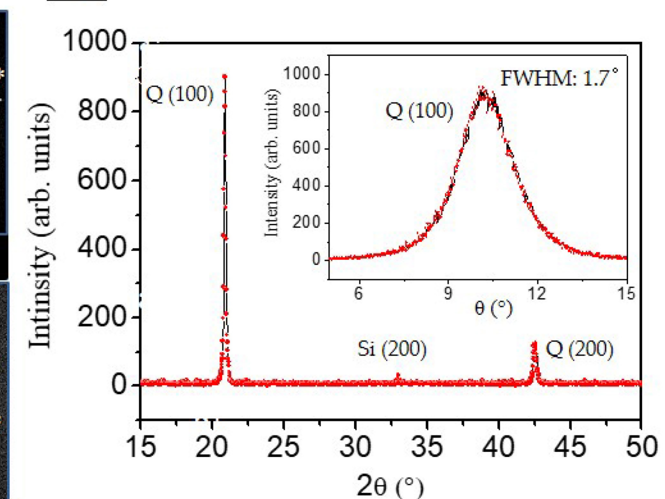

a

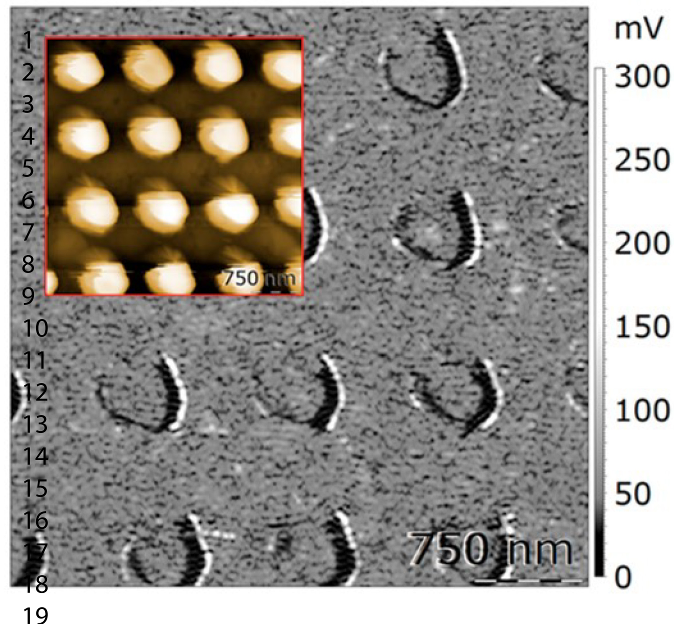

1
2
3
4
5
6
7
8
9
10
11
12
13
14
15
16
17
18
19

b

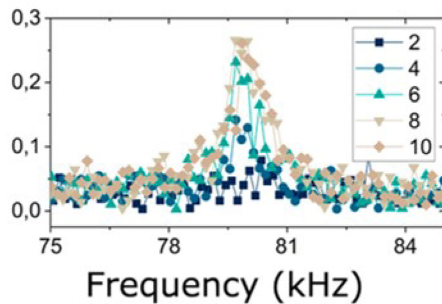

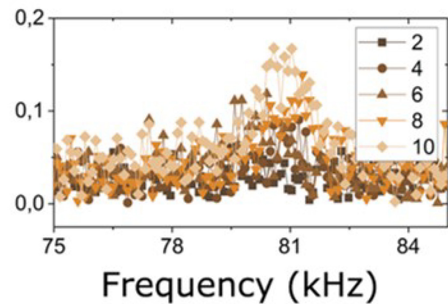

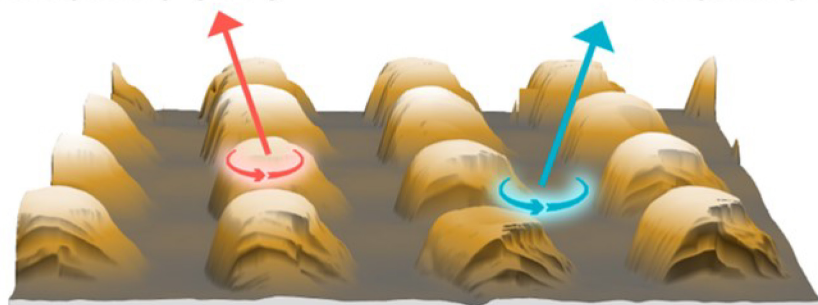

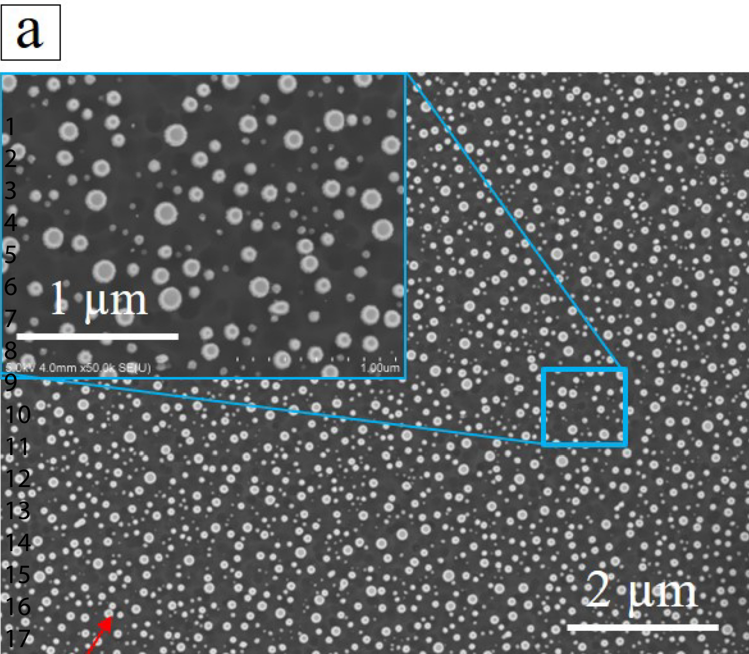

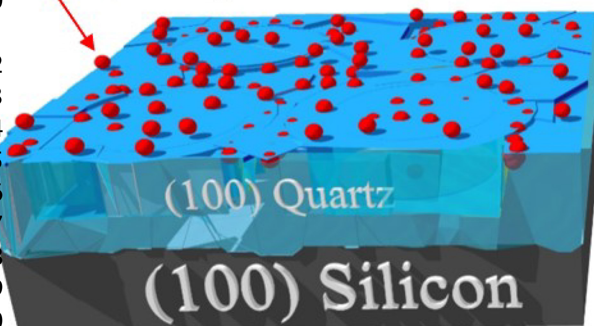

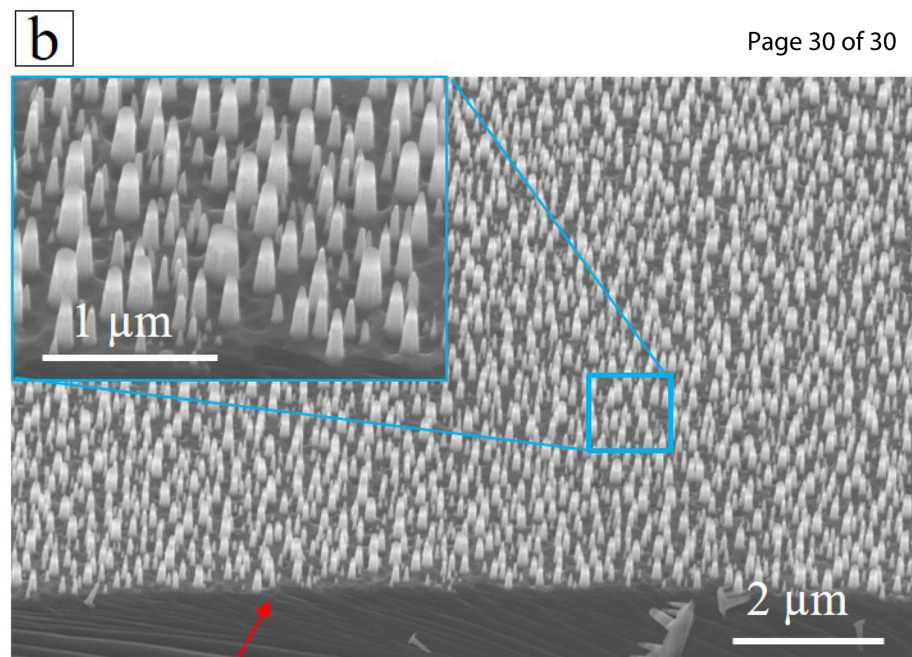

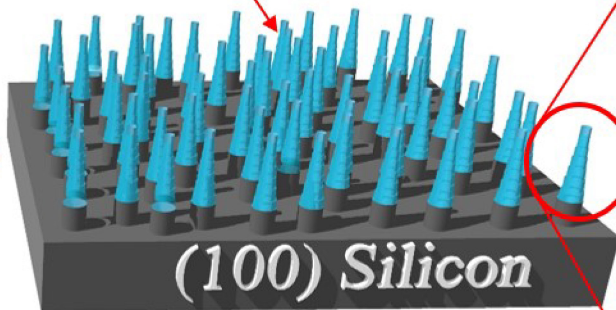

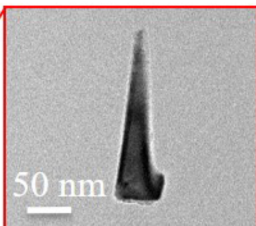

1
2
3
4
5
6
7
8
9
10
11
12
13
14
15
16
17
18
19
20
21
22
23
24
25
26
27
28
29
30
31
32